

Experimental investigation of a quantum Otto heat engine with shortcuts to adiabaticity implemented using counter-adiabatic driving

Krishna Shende,^{1,*} Matreyee Kandpal,^{1,†} Arvind,^{1,‡} and Kavita Dorai^{1,§}

¹*Department of Physical Sciences, Indian Institute of Science Education & Research Mohali, Sector 81 SAS Nagar, Manauli PO 140306 Punjab India.*

The finite time operation of a quantum Otto heat engine leads to a trade-off between efficiency and output power, which is due to the deviation of the system from the adiabatic path. This trade-off caveat can be bypassed by using the shortcut-to-adiabaticity protocol. We experimentally implemented a quantum Otto heat engine using spin-1/2 nuclei on a nuclear magnetic resonance (NMR) quantum processor. We investigated its performance using the shortcut-to-adiabaticity technique via counter-adiabatic driving with the inclusion of the cost to perform the shortcut. We use two different metrics that incorporate the cost of shortcut-to-adiabaticity to define engine efficiency and experimentally analyze which one is more appropriate for the NMR platform. We found a significant improvement in the performance of the quantum Otto heat engine driven by shortcut-to-adiabaticity, as compared to the non-adiabatic heat engine.

I. INTRODUCTION

One of the fundamental results of thermodynamics is that the efficiency of any heat engine with hot and cold reservoirs (at temperature T_h and T_c , respectively), is limited by the Carnot efficiency ($\eta_C = 1 - T_c/T_h$). Since physical heat engines have a finite operation cycle time, they are not in an exact equilibrium state during operation, and hence do not satisfy the quasi-static process condition. Consequently, their efficiency is always lower than the maximum achievable Carnot efficiency. Quantum thermodynamics, which deals with the thermodynamics of quantum systems, has made rapid progress in recent years and fluctuation theorems and thermodynamic uncertainty relations have been discovered [1, 2]. A heat engine operating on the quantum scale is called a quantum heat engine (QHE), and experimental implementations of QHEs have been reported in NMR [3–5], superconducting qubits[6], NV centers [7] and ion traps [8, 9]. A QHE has been proposed with an Ising spin chain as the working material [10, 11], the effect of coherence in QHEs has been studied[12], and an engine driven by quantum coherence has been proposed [13].

The working of the QHE is based on the assumption that ideal adiabatic transformations are quasi-static, which implies that the QHE cycle time is infinitely long, to achieve an ideal process. In real life, QHEs are implemented in a finite time, which leads to irreversibility, which can be quantified as irreversible work and inner friction in the thermodynamic process [14]. The non-commutativity of the driving Hamiltonian at different times induces transitions among the instantaneous energy eigenstates, which is classified as quantum friction [15–17]. The finite time operation of a practical QHE

and extra coherence build up due to non-commutativity of Hamiltonian leads to a trade-off between power and efficiency, such that an increase in efficiency leads to a decrease in power and vice versa.

A long standing hurdle in experimental implementations of QHEs is to design an efficient QHE which can deliver more output in a finite operation time. A new quantum control protocol, called short to adiabaticity(STA) was proposed to overcome this difficulty [18–21]. In an STA protocol, a quantum adiabatic process is mimicked in a finite amount of time such that there is no transition between the energy eigen states during the transformation and thus the system follows an adiabatic path. Various approaches to implement STA have been proposed, including via counter-adiabatic driving, where an extra term is added to the original Hamiltonian which keeps the system on an adiabatic path and suppresses the non-adiabatic transitions [22–25]. STA has been successfully implemented experimentally on various quantum processing platforms such as superconducting qubits[26], Bose-Einstein condensate[27], NV centers[28], cold atoms[29], trapped ions[30] and NMR[31].

In this work, we use counter-adiabatic driving in a spin-1/2 Landau-Zener(LZ) model of a quantum Otto heat engine to implement STA, and explore its performance on an NMR quantum processor. We experimentally implement the engine cycles using two qubits for two different sets of reservoir temperatures. We also compared the figures of merit of the quantum Otto heat engine, implemented with and without STA, in order to investigate the dynamics of efficiency and power. Engine efficiency was calculated by taking into account STA driving costs. We computed engine efficiency using two different definitions that incorporate the STA cost, and experimentally determine the definition which is useful for the NMR platform. Our experimental results conclude that the quantum Otto heat engine performs better with STA driving as compared to the nonadiabatic quantum heat engine.

The rest of this paper is organized as follows: Section II

* ph19032@iisermohali.ac.in

† ph23022@iisermohali.ac.in

‡ arvind@iisermohali.ac.in

§ kavita@iisermohali.ac.in

contains a brief description of the requisite theoretical background, with Sections II A-II C describing the quantum Otto heat engine, the basics of counter-adiabatic driving, and the engine model, respectively. Section III describes the experimental implementation of the heat engine. Section IV contains a discussion of the main results, while Section V offers some concluding remarks.

II. THEORETICAL BACKGROUND

A. Quantum Otto heat engine

The quantum Otto heat engine cycle is a four stroke cycle operating between a hot and a cold reservoir. Two strokes are isochoric and two strokes are adiabatic. The isochoric processes are carried out by thermalizing the system with a hot or a cold reservoir, as needed. The adiabatic processes comprise of an expansion and a compression and are carried out by changing the time-dependent parameter($\lambda(t)$) of the system Hamiltonian $H_0(\lambda(t))$. The schematic diagram of quantum Otto heat engine cycle is shown in Figure.1.

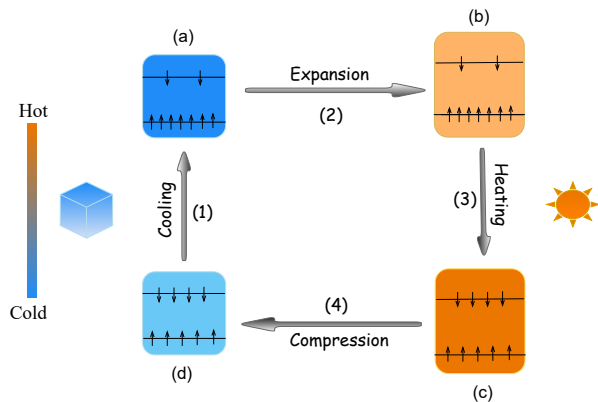


FIG. 1. Schematic representation of a quantum Otto heat engine cycle. (1) and (3) are cooling and heating strokes which are implemented by establishing contact between a hot and a cold bath respectively, which results in a change in the populations of the working system. (2) and (4) are expansion and compression strokes which are realized by changing the energy gap of the working system.

(i) *Cooling*: At first, the working medium is brought in contact with a cold bath at inverse temperature β_C such that it is equilibrated to a state $\rho_a = e^{-\beta_C H(\lambda_1)} / Z_1$, where $H(\lambda_1)$ is the system Hamiltonian and Z_1 is the partition function. The cold inverse temperature has the form $\beta_C = 1/k_B T_C$, where k_B is the Boltzmann constant and T_C is the cold bath temperature.

(ii) *Expansion*: In this step, the system is separated from bath and the Hamiltonian parameter is changed from $H(\lambda_1)$ at time $t=0$ to $H(\lambda_2)$ till time $t=\tau$ using a unitary transformation. This increases the energy gap between

the working medium adiabatically and is assumed to be ideal, such that no unwanted transitions occur during evolution.

(iii) *Heating*: Again, contact between the hot bath at inverse temperature β_H and the working medium is established, such that the system thermalizes to a state $\rho_c = e^{-\beta_H H(\lambda_2)} / Z_2$, where Z_2 is the partition function.

(iv) *Compression*: In this step, the time dependent Hamiltonian parameter $\lambda(t)$ of the working medium is changed from λ_2 to λ_1 under a unitary evolution.

The average work performed during unitary adiabatic driving i.e. expansion or compression is given by [1, 2]:

$$\langle W \rangle = Tr[H_f \rho_f] - Tr[H_i \rho_i] \quad (1)$$

where H_i and ρ_i are the initial Hamiltonian and density matrix immediately after the thermalization step, and H_f and ρ_f are the final Hamiltonian and the density matrix after the expansion or compression process.

The average heat exchange between the reservoir and the system is given as:

$$\langle Q \rangle = Tr[H' \rho'_f] - Tr[H' \rho'_i] \quad (2)$$

where H' is the system Hamiltonian during the thermalization process, which remains constant; ρ'_i and ρ'_f are the density matrix before and after the thermalization process, respectively.

B. Counter-adiabatic driving

When a system evolves under a time dependent Hamiltonian $H_0(t)$, the Hamiltonian must vary slowly enough so that the system evolves adiabatically and remains in the instantaneous eigen state of the Hamiltonian. A Hamiltonian not obeying the adiabaticity condition will induce unwanted transitions during the evolution. These unwanted transitions can be avoided by using an STA technique such as counter-adiabatic Driving(CD) [24, 25]. In this method, an additional term ($H_{CD}(t)$) is added to the original Hamiltonian($H_0(t)$):

$$H(t) = H_0(t) + H_{CD}(t) \quad (3)$$

The CD scheme ensures that the system remains in the instantaneous eigenstates of the original Hamiltonian $H_0(t)$ when it is driven using the new effective Hamiltonian $H(t)$. Hence, the system follows an adiabatic path. The exact form of $H_{CD}(t)$ is given by [24]:

$$H_{CD}(t) = i\hbar \sum_n (|\partial_t n\rangle \langle n| - |n\rangle \langle \partial_t n|) \quad (4)$$

where $|n\rangle = |n(t)\rangle$ is the n^{th} eigenstate of the original Hamiltonian $H_0(t)$, at time t .

C. Engine model

For a spin-1/2 system placed in an arbitrary magnetic field and assuming a Landau-Zener type model, the original Hamiltonian is given by [32]:

$$H_0(t) = b_x \sigma_x + b_z(t) \sigma_z \quad (5)$$

where b_x and $b_z(t)$ are external magnetic fields, b_x is the minimum splitting frequency between energy levels, $b_z(t)$ is the time-dependent external field and $\sigma_{x,z}$ are the Pauli matrices. The CD Hamiltonian assumes the form:

$$H_{CD}(t) = -\frac{b_x \dot{b}_z}{2[b_x^2 + b_z^2]} \sigma_y = b_{CD}(t) \sigma_y \quad (6)$$

The form of $b_j(t)$ is given by [33]:

$$b_j(t) = C_j + D_j \frac{t^2}{\tau^2} \left(\frac{1}{2} - \frac{t}{3\tau} \right) \quad (7)$$

where C_j and D_j are arbitrary constants that determine the initial and final values of the external driving frequency, j is either x or y, τ is the total driving time and $t \in [0, \tau]$. The CD Hamiltonian H_{CD} must vanish at the beginning and at the end of the driving time, which imposes the conditions $b_{CD}(t=0, \tau)=0$ and $\dot{b}_{CD}(t=0, \tau)=0$. The form of Eq.7 already takes care of the above boundary conditions, and hence can be used for STA driving.

The performance of a heat engine is quantified by its working efficiency and output power. Engine efficiency is quantified by the net output work performed by the working medium divided by the heat transferred from the hot bath, giving the fraction of heat energy converted into work. Output power is the rate at which output energy is produced. Ideally, for an adiabatic cycle, the efficiency and power are given by:

$$\eta_A = -\frac{\langle W_2 \rangle + \langle W_4 \rangle}{\langle Q_3 \rangle} \quad \& \quad P_A = -\frac{\langle W_2 \rangle + \langle W_4 \rangle}{\tau_{cycle}} \quad (8)$$

where η_A and P_A are the adiabatic efficiency and power respectively, $\langle W_2 \rangle$ and $\langle W_4 \rangle$ denote average work performed during the expansion and compression steps, $\langle Q_3 \rangle$ is the average heat absorbed during the isochoric heating step, and τ_{cycle} is the cycle duration.

For an STA heat engine, an extra term has been added to the original Hamiltonian to enhance its overall working dynamics. Hence, this extra input energy needs to be considered in the performance of the STA heat engine.

The first definition of the efficiency of the STA engine is given by [21, 33, 34]:

$$\eta_{STA}^1 = -\frac{\langle W_2 \rangle^{STA} + \langle W_4 \rangle^{STA}}{\langle Q_3 \rangle + \langle \dot{H}_2 \rangle_\tau^{STA} + \langle \dot{H}_4 \rangle_\tau^{STA}} \quad (9)$$

Similarly, the second definition for the efficiency of the STA engine has been proposed in Ref. [35] as:

$$\eta_{STA}^2 = -\frac{\langle W_2 \rangle^{STA} + \langle W_4 \rangle^{STA} + \langle \dot{H}_2 \rangle_\tau^{STA} + \langle \dot{H}_4 \rangle_\tau^{STA}}{\langle Q_3 \rangle} \quad (10)$$

and the power is given by:

$$P_{STA} = -\frac{\langle W_2 \rangle^{STA} + \langle W_4 \rangle^{STA} - \langle \dot{H}_2 \rangle_\tau^{STA} - \langle \dot{H}_4 \rangle_\tau^{STA}}{\tau_{cycle}} \quad (11)$$

where STA denotes quantities that define the STA heat engine and the cost of the STA implementation during an adiabatic process is given by [33]:

$$\langle \dot{H}_i \rangle^{STA} = \int_0^\tau \langle \dot{H}_{CD}(t) \rangle^{STA} dt \quad (12)$$

which is the time average of the energy spent to implement STA ($i = 2, 4$), and H_{CD} is the form of the CD Hamiltonian during expansion or compression. The above equations define the energy required to maintain an adiabatic path during expansion and compression.

III. EXPERIMENTAL IMPLEMENTATION

A. Experimental details

In our experiments, we have used $^{13}\text{C}_2$ -labeled Glycine where the $^{13}\text{C}_1$ and $^{13}\text{C}_2$ spins are encoded as the first and second qubits, respectively. The molecular structure and system parameters including the chemical shifts ν_i and the scalar coupling constant J are given in Fig. 2. The rotating frame Hamiltonian for two spin-1/2 nuclei is given by [36]:

$$\mathcal{H} = -\hbar \sum_{i=1}^2 \omega_i I_z^i + \hbar \sum_{i<j=1}^2 J_{ij} I_z^i I_z^j \quad (13)$$

where ω_i the offset angular frequency of the i^{th} nucleus, I_z^i represents the z-component of the spin angular momentum of the i^{th} nucleus and J_{ij} is the scalar coupling between the i^{th} and the j^{th} nuclei. All the experiments were performed at room temperature on a Bruker Avance III 600-MHz FT-NMR spectrometer equipped with a QXI probe. The measured T_1 and T_2 relaxation times for $^{13}\text{C}_1$ and $^{13}\text{C}_2$ spins are 28.57 s and 3.28 s and are 1.84 s and 1.25 s, respectively.

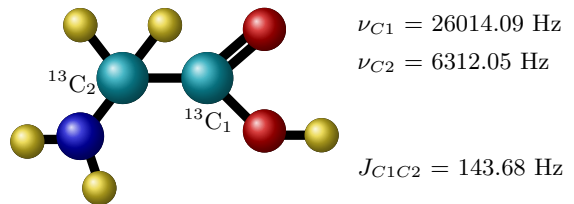


FIG. 2. Molecular structure of $^{13}\text{C}_2$ -labeled glycine with the $^{13}\text{C}_1$ and $^{13}\text{C}_2$ nuclei encoded as the first and second qubits, respectively. The scalar coupling strength and the offset rotation frequencies, are listed alongside.

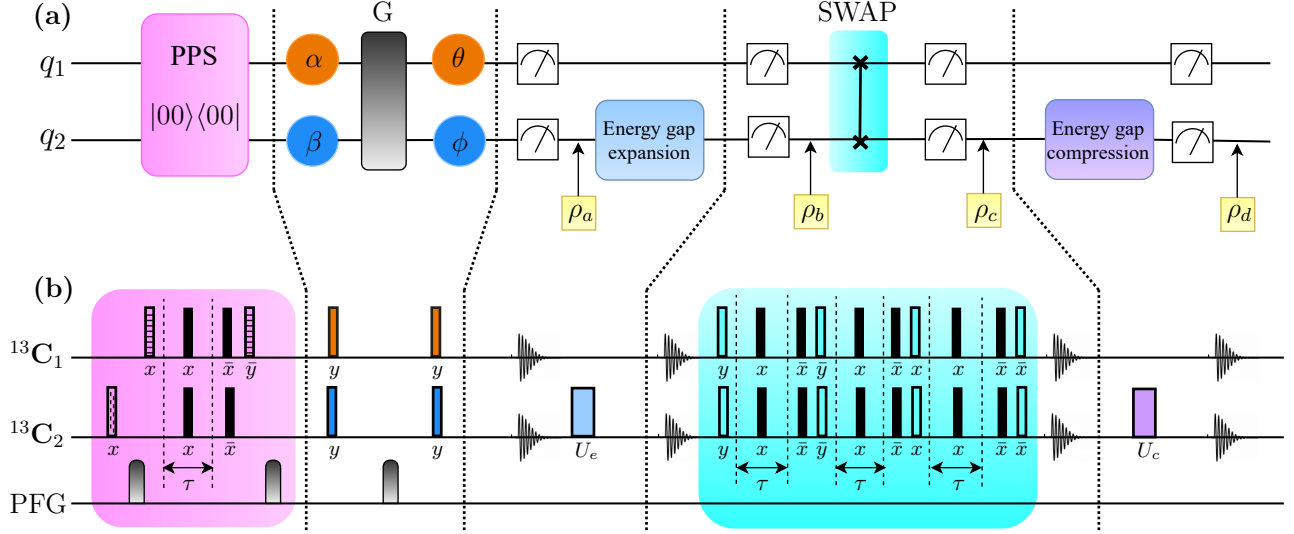


FIG. 3. (a) Schematic circuit diagram to realize QOHE using a two-qubit system in NMR. (b) NMR pulse sequence to implement the Otto heat engine. Bars containing dashed vertical lines, bars with horizontal lines, unfilled and filled bars represent $(\frac{\pi}{3})$, $(\frac{\pi}{4})$, $(\frac{\pi}{2})$ and (π) rotation angles respectively, with their corresponding rotation axis given below each bar. Orange and blue bars represent pulses used to initialize hot and cold bath temperatures, respectively. Cyan and violet bars depict external driving expansion (U_e) and compression (U_c) unitary pulses, respectively. The line depicting application of a pulsed field gradient (PFG) marks the times at which a gradient is employed to destroy coherence. The time delay τ is set equal to $\frac{1}{2J_{C_1 C_2}}$.

The complete circuit diagram and pulse sequence to perform the study of non-equilibrium dynamics is shown in Fig.3. The spatial averaging technique[37] has been used to initialize the system in a pseudopure state $|00\rangle\langle 00|$ with the corresponding density operator given by:

$$\rho_{00} = \frac{1 - \epsilon}{4} I_4 + \epsilon |00\rangle\langle 00| \quad (14)$$

where I_4 is the 4×4 identity operator and ϵ is proportional to the spin polarization ($\approx 10^{-5}$ at room temperature). The circuit and pulse sequence used to achieve this are shown in the pink shaded portion of Fig. 3. We have used the Gradient Ascent Pulse Engineering (GRAPE) technique[38] for the optimization of all the radiofrequency (RF) pulses used to construct the pseudopure state. The GRAPE optimized RF pulses are robust against RF inhomogeneity, with an average fidelity of 0.999. All the $\frac{\pi}{2}$ pulses used to create the pseudopure state have a duration of 150 μ s with a maximum power level of 179.47 W for the QXI probe.

We performed full quantum state tomography to reconstruct the experimental matrix. The closeness between the theoretical and experimental states is quantified using the fidelity measure [39, 40]:

$$F = \frac{|Tr(\rho_e \rho_t^\dagger)|}{\sqrt{Tr(\rho_e \rho_e^\dagger) Tr(\rho_t \rho_t^\dagger)}} \quad (15)$$

where ρ_t and ρ_e are the theoretically predicted and experimentally measured density matrices, respectively.

B. Experimental implementation of the Otto engine

We used the $^{13}C_2$ (second qubit) as the working medium and the $^{13}C_1$ (first qubit) as the auxiliary qubit to implement the isochoric heating stroke. The first stroke of the QHE initializes the qubits to the desired spin temperature, such that the working qubit is at a cold spin temperature and the auxiliary qubit is at a hot spin temperature. The effective spin temperature (β) of the initial Gibbs state is related to the ground state (p_0) and the excited state (p_1) populations as[4]:

$$\frac{1}{k_B T} = \beta = \frac{1}{h\nu_i} \ln \left(\frac{p_0}{p_1} \right) \quad (16)$$

where h is Planck's constant, k_B is Boltzmann's constant, T is the spin temperature and ν is the frequency of the energy gap. By applying an RF pulse of an appropriate angle of rotation (between 0 and π) to the pseudopure state, the populations are redistributed between the qubit states and coherence is created. A pulsed field gradient (PFG) is employed to destroy unwanted coherence and achieve the final desired thermal state. Thus, each qubit is equilibrated at different "pseudo-spin" temperatures. We perform quantum state tomography to reconstruct the final state and to verify that the system

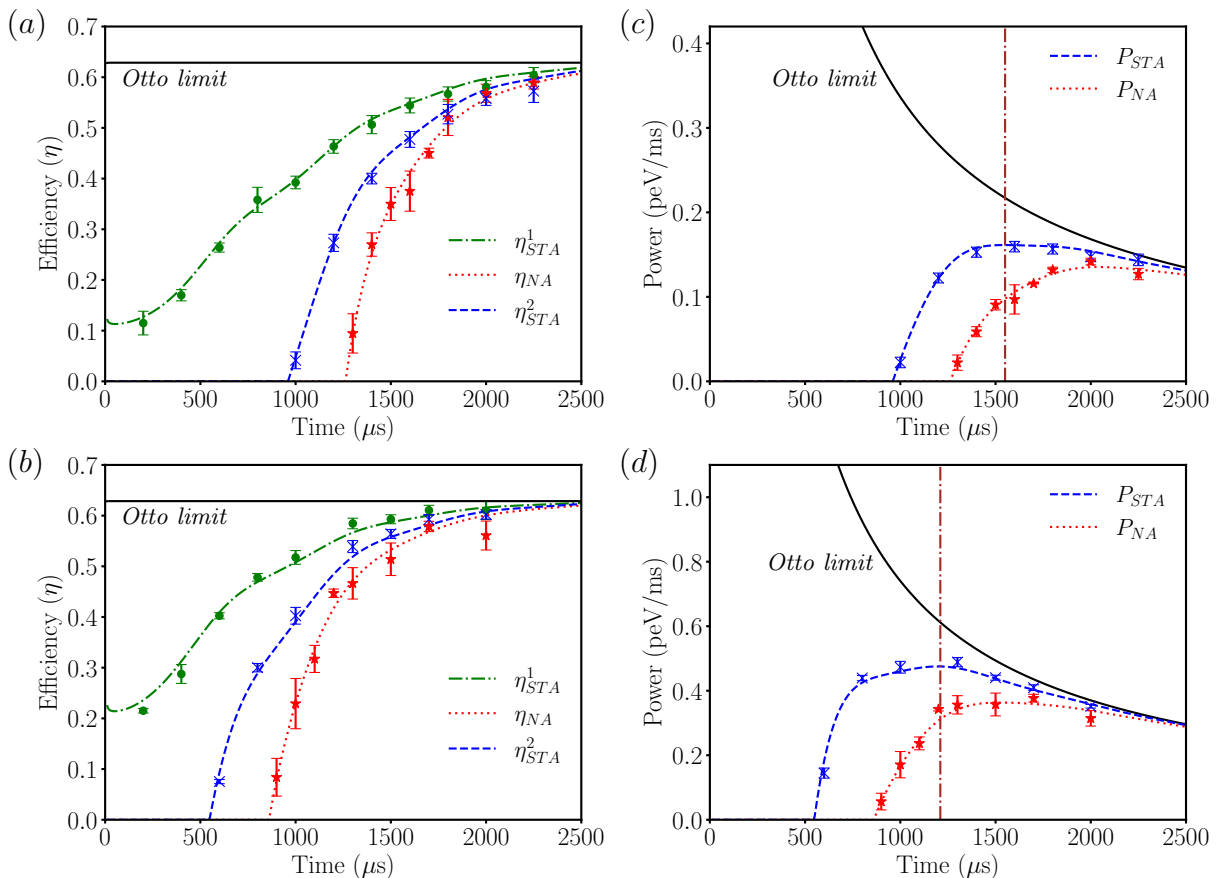


FIG. 4. Quantum Otto heat engine dynamics: Efficiency((a)-(b)) and output power((c)-(d)) as a function of driving time(τ). Solid black lines mark the theoretical prediction, while dashed blue, dot-dashed green and dotted red curves are from the simulations. Points marked with blue crosses, green circles and red stars (along with error bars) represent experimental data. The cold source spin temperature is set to $k_B T_C = 11.94$ peV. Plots in the upper and lower panels correspond to hot spin temperatures of $k_B T_H^1 = 40.54$ peV and $k_B T_H^2 = 53.11$ peV, respectively. The driving time at which maximum power is obtained is marked by a dot-dashed vertical line.

is initialized to the required thermal state. We initialized the working qubit to a cold spin temperature of $k_B T_C = 11.94$ peV and the auxiliary qubit to spin temperatures of $k_B T_H^1 = 6.45$ peV and $k_B T_H^2 = 8.45$ peV, respectively.

During expansion, the original Hamiltonian for the system is given by:

$$\mathcal{H}_0^{\text{exp}}(t) = \frac{\hbar}{2} 2\pi [\nu_x \sigma_x + \nu_z(t) \sigma_z] \quad (17)$$

with $\nu_z(t) = D_{\text{exp}} \frac{t^2}{\tau^2} \left(\frac{1}{2} - \frac{t}{3\tau} \right)$. The RF field intensity is adjusted such that $\nu_x = 1000$ Hz and $\nu_z(t)$ changes from 0 Hz at $t=0$ to 2500 Hz at $t=\tau$. The driving time τ is varied in this interval from 200 to 2250 μ s. The H_{CD} term to perform STA during expansion is given by Eq.6, using the ν_x and $\nu_z(t)$ given above. This driving time is much shorter than the decoherence time (which is in the order of seconds) and hence the driving process can be considered to be a unitary evolution $U_{\tau,0}$ [3, 41]. The

expansion stroke is implemented by applying a unitary GRAPE pulse (with a fidelity ≥ 0.999) of duration varying from 600 μ s to 6000 μ s.

The isochoric heating stroke is performed by emulating the heat exchange between the working system and the bath using the $^{13}\text{C}_1$ spin, which was initially prepared in a pseudothermal state with inverse spin temperature β_H . The thermalization process is achieved by applying a SWAP gate between the working and the auxiliary qubits (depicted in the blue shaded portion of Fig. 3).

The compression stroke is realized by implementing the following Hamiltonian:

$$\mathcal{H}_0^{\text{comp}}(t) = \mathcal{H}_0^{\text{exp}}(t) \quad (18)$$

with $\nu_z(t) = C_{\text{comp}} + D_{\text{comp}} \frac{t^2}{\tau^2} \left(\frac{1}{2} - \frac{t}{3\tau} \right)$, such that $\nu_z(t)$ changes from 2500 Hz at $t=0$ to 0 Hz at $t=\tau$ and H_{CD} changes accordingly. GRAPE pulses have been used to implement the compression stroke operations. The total duration of the heat engine operation is less than 30

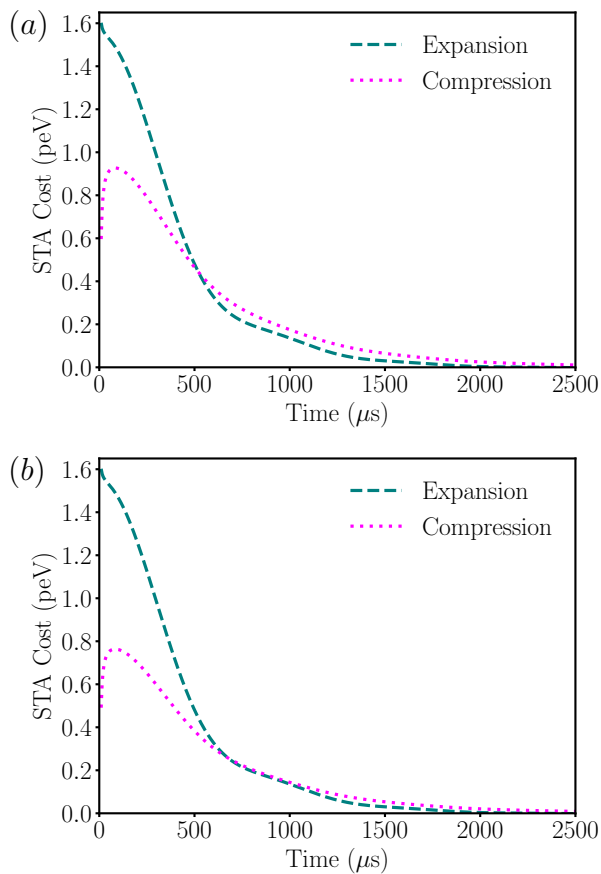


FIG. 5. Quantum Otto Engine STA cost dynamics: The theoretically calculated STA cost for the expansion and compression processes is depicted using dashed teal and dotted magenta lines, respectively, as a function of the driving time (τ). The cold source spin temperature is fixed at $k_B T_C = 1.9$ peV. The upper and lower plots correspond to hot spin temperatures of $k_B T_{H1} = 6.45$ peV and $k_B T_{H2} = 8.45$ peV, respectively.

ms, which is well below the transverse relaxation time for both the nuclear spins. We have chosen the spin temperatures and the energy gap frequencies such that the heat engine working condition [42]:

$$\frac{T_H}{T_C} > \frac{\nu_f}{\nu_i} \quad (19)$$

is satisfied, where T_H and T_C are the hot and cold bath temperatures respectively, and $\nu_i = 1000$ Hz and $\nu_f = 2692.6$ Hz are the minimum and maximum energy gap frequencies, respectively. The maximum achievable efficiency for the heat engine operation is given as:

$$\eta = 1 - \frac{\nu_i}{\nu_f}. \quad (20)$$

Using these values of the maximum and minimum energy gap, we obtain the Otto limit efficiency of ≈ 0.629 .

IV. RESULTS & DISCUSSION

The dynamics of the quantum Otto heat engine was studied using an LZ type model, by changing the driving time (τ) for the adiabatic process and the hot source temperature, such that the cold bath temperature is kept fixed. The working qubit $^{13}\text{C}_2$ is initialized to a cold spin temperature $k_B T_C = 1.9$ peV, while the auxiliary qubit $^{13}\text{C}_1$ was prepared at two different hot spin temperatures $k_B T_{H1} = 6.45$ peV and $k_B T_{H2} = 8.45$ peV, to carry out two different sets of experiments. The fidelity of the experimentally prepared quantum states at each temperature was verified via quantum state tomography.

The performance of a QHE can be analyzed through the behavior of its efficiency and the output power delivered. Figure 4 depicts these figures of merit, with the hot reservoir temperature being kept at 6.45 peV and 8.45 peV respectively, while keeping the cold reservoir temperature fixed. The engine efficiency at different driving times (τ) is shown in Figure 4(a)-(b), where the maximum achievable efficiency i.e. the Otto limit (≈ 0.629) is shown by a solid black line. Dashed blue, dotted-dashed green and dotted red curves represent the theoretically predicted efficiencies for different driving times of the STA and non-adiabatic (NA) heat engines respectively, while the experimentally obtained values with error bars for each heat engine are plotted with the same color code. We observed that for smaller driving times the NA heat engine does not produce any useful work as the entropy production is very high. As we increase the driving time, the irreversible entropy production is reduced, and after $\approx 1300 \mu\text{s}$ and $\approx 900 \mu\text{s}$ for T_{H1} and T_{H2} respectively, useful work is extracted and the efficiency is positive. If the driving time is increased gradually, the efficiency reaches the Otto limit, which is due to the fact that the process is getting closer to the ideal adiabatic process, since a decrease in the entropy production leads to an increase in the efficiency.

The theoretically calculated efficiency of STA engine using both definitions (Eqs.9 and 10) is shown in Figs. 4 (a) and (b) (dot-dashed green and dashed blue curves). We observed that if we use the first definition of efficiency, the efficiency even at low driving times is positive, which implies a certain amount of work can be extracted, leading to a positive output power. However, for low driving times there is no output power, hence we conclude that the first definition of efficiency is not relevant for our experiments. On the other hand, using the second definition of efficiency ensures that for low driving times, both the efficiency and power are zero and this definition hence correctly captures the STA engine dynamics.

We note here in passing that, if we use the second definition of efficiency (Eq.9), then both the STA heat engine plots retain a finite amount of efficiency for small driving times such as $10 \mu\text{s}$. This indicates the supremacy of the STA protocol over the normal NA driving protocol. The STA efficiency saturates to the Otto limit when driving time is enhanced. The STA heat engine efficiency is al-

ways greater than the NA heat engine efficiency, until the point where they both merge and become equal to the Otto limit at very high driving times.

Figs. 4(c) and (d) display the power for various driving times. Black, blue and red curves are for theoretically calculated values of power for adiabatic, STA, and NA heat engines, respectively. The experimental power values corresponding to STA and NA heat engines are plotted with the designated color along with error bars. We obtained a good match between experimental data and theoretical calculations. The efficiency trend has been followed by power as well, as we observe that the STA heat engine power is always greater than the NA heat engine power. The vertical brown dashed-dotted line marks the driving time at which the output power is maximum for STA heat engine. We obtained maximum power at $1550 \mu s$ and $1210 \mu s$ for the STA heat engine when the hot reservoir temperature is kept at T_{H1} and T_{H2} , respectively. We achieved maximum power at $2000 \mu s$ and $1500 \mu s$ for the NA heat engine (not shown in the plots), when the hot reservoir temperature is kept at T_{H1} and T_{H2} , respectively. Therefore, we obtain more power for smaller driving times for the STA heat engine, which implies that the overall performance of the STA heat engine is better than the NA heat engine even after spending an extra amount of energy to maintain the adiabatic path. We observed that at low driving times, the output power is zero for the STA heat engine even though the efficiency is non-zero, which is due to the definition of power for the STA heat engine. The STA cost is significantly high at lower driving times, which is subtracted from the output work in Eq.11. Hence, the power becomes zero at low driving times and it becomes positive only after the STA cost is reduced to a certain level after a particular driving time.

The addition of an extra term in the original Hamiltonian to implement STA via counter-adiabatic driving requires an additional amount of energy termed the ‘STA cost’ for the expansion and compression processes. This extra cost can be calculated according to Eq.12, and Fig.5(a)-(b) shows the theoretically calculated STA cost during the expansion and compression operations for two different sets of reservoir temperatures. We observed that the STA cost for expansion is the same in both the plots as the cold reservoir temperature and initial and final energy gaps are fixed. The STA cost for compression is smaller for higher hot source temperatures ($T_{H2} > T_{H1}$) as compared to lower hot source temperatures. Hence, this reduction in STA cost gets reflected in the efficiency, and the efficiency at small driving times for higher hot source temperatures is more than the lower hot source

temperatures. One possible explanation of having higher STA cost for expansion is the fact that the population difference between the two states is high system state is initialized to cold spin temperatures, which increases the probability of transitions between the states. Hence, more amount of energy is required to maintain the population difference throughout the adiabatic expansion operation. When the system starts from a hot spin temperature, the population difference between the higher and lower energy states is less than that for cold spin temperature systems. Hence the transition probability between the states is reduced. Therefore, less amount of energy is spent to maintain the population difference during the compression operation. As $T_{H2} > T_{H1}$, the STA cost for compression is less when the hot reservoir is at T_{H2} as compared to T_{H1} . This could be due to the fact that T_{H2} has lower population difference as compared to T_{H2} .

V. CONCLUSIONS

We experimentally implemented an STA protocol based on the counter-adiabatic driving technique for a LZ model quantum Otto heat engine on an NMR quantum processor. We used different hot source spin temperatures and driving times to investigate the performance of the quantum Otto heat engine by taking into account the extra STA cost which has been spent to keep the system in quasi-static equilibrium. We compared two different definitions of efficiency for the STA engine and argued the correctness of one definition over the other. It can be concluded from figures of merit such as efficiency and power that the performance of the STA heat engine is superior to the non-adiabatic heat engine, as it can deliver more output power in less driving time. Our results are a step forward in the direction of improving the performance and efficiency of physical realizations of quantum heat engines.

ACKNOWLEDGMENTS

All experiments were performed on a Bruker Avance-III 600 MHz FT-NMR spectrometer at the NMR Research Facility at IISER Mohali. K.S. acknowledges financial support from the Prime Minister’s Research Fellowship(PMRF) scheme of the Government of India. M.K. acknowledges financial support from DST-INSPIRE fellowship.

-
- [1] S. Deffner and S. Campbell, *Quantum Thermodynamics*, 2053-2571 (Morgan & Claypool Publishers, 2019).
 [2] S. Vinjanampathy and J. Anders, *Contemporary Physics* **57**, 545 (2016).

- [3] J. P. S. Peterson, T. B. Batalhão, M. Herrera, A. M. Souza, R. S. Sarthour, I. S. Oliveira, and R. M. Serra, *Phys. Rev. Lett.* **123**, 240601 (2019).

- [4] R. J. de Assis, T. M. de Mendonça, C. J. Villas-Boas, A. M. de Souza, R. S. Sarthour, I. S. Oliveira, and N. G. de Almeida, *Phys. Rev. Lett.* **122**, 240602 (2019).
- [5] V. F. Lisboa, P. R. Dieguez, J. R. Guimarães, J. F. G. Santos, and R. M. Serra, *Phys. Rev. A* **106**, 022436 (2022).
- [6] A. Solfanelli, A. Santini, and M. Campisi, *PRX Quantum* **2**, 030353 (2021).
- [7] J. Klatzow, J. N. Becker, P. M. Ledingham, C. Weinzetl, K. T. Kaczmarek, D. J. Saunders, J. Nunn, I. A. Walmisley, R. Uzdin, and E. Poem, *Phys. Rev. Lett.* **122**, 110601 (2019).
- [8] J. Roßnagel, S. T. Dawkins, K. N. Tolazzi, O. Abah, E. Lutz, F. Schmidt-Kaler, and K. Singer, *Science* **352**, 325 (2016).
- [9] G. Maslennikov, S. Ding, R. Hablützel, J. Gan, A. Roulet, S. Nimmrichter, J. Dai, V. Scarani, and D. Matsukevich, *Nature Communications* **10**, 202 (2019).
- [10] G. Piccitto, M. Campisi, and D. Rossini, *New Journal of Physics* **24**, 103023 (2022).
- [11] R. B.S, V. Mukherjee, and U. Divakaran, *Entropy* **24** (2022), 10.3390/e24101458.
- [12] P. A. Camati, J. F. G. Santos, and R. M. Serra, *Phys. Rev. A* **99**, 062103 (2019).
- [13] S. Aimet and H. Kwon, *Phys. Rev. A* **107**, 012221 (2023).
- [14] F. Plastina, A. Alecce, T. J. G. Apollaro, G. Falcone, G. Francica, F. Galve, N. Lo Gullo, and R. Zambrini, *Phys. Rev. Lett.* **113**, 260601 (2014).
- [15] T. Feldmann and R. Kosloff, *Phys. Rev. E* **73**, 025107 (2006).
- [16] G. Thomas and R. S. Johal, *The European Physical Journal B* **87**, 166 (2014).
- [17] R. Kosloff and T. Feldmann, *Phys. Rev. E* **65**, 055102 (2002).
- [18] X. Chen, A. Ruschhaupt, S. Schmidt, A. del Campo, D. Guéry-Odelin, and J. G. Muga, *Phys. Rev. Lett.* **104**, 063002 (2010).
- [19] X. Chen, I. Lizuain, A. Ruschhaupt, D. Guéry-Odelin, and J. G. Muga, *Phys. Rev. Lett.* **105**, 123003 (2010).
- [20] D. Guéry-Odelin, A. Ruschhaupt, A. Kiely, E. Torrontegui, S. Martínez-Garaot, and J. G. Muga, *Rev. Mod. Phys.* **91**, 045001 (2019).
- [21] O. Abah and E. Lutz, *Phys. Rev. E* **98**, 032121 (2018).
- [22] M. Demirplak and S. A. Rice, *The Journal of Physical Chemistry A* **107**, 9937 (2003).
- [23] M. Demirplak and S. A. Rice, *The Journal of Physical Chemistry B* **109**, 6838 (2005).
- [24] M. V. Berry, *Journal of Physics A: Mathematical and Theoretical* **42**, 365303 (2009).
- [25] K. Takahashi, *Phys. Rev. E* **87**, 062117 (2013).
- [26] K. Funo, N. Lambert, B. Karimi, J. P. Pekola, Y. Masuyama, and F. Nori, *Phys. Rev. B* **100**, 035407 (2019).
- [27] M. G. Bason, M. Viteau, N. Malossi, P. Huillery, E. Arimondo, D. Ciampini, R. Fazio, V. Giovannetti, R. Mannella, and O. Morsch, *Nature Physics* **8**, 147 (2012).
- [28] J. Zhang, J. H. Shim, I. Niemeyer, T. Taniguchi, T. Teraji, H. Abe, S. Onoda, T. Yamamoto, T. Ohshima, J. Isoya, and D. Suter, *Phys. Rev. Lett.* **110**, 240501 (2013).
- [29] Y.-X. Du, Z.-T. Liang, Y.-C. Li, X.-X. Yue, Q.-X. Lv, W. Huang, X. Chen, H. Yan, and S.-L. Zhu, *Nature Communications* **7**, 12479 (2016).
- [30] S. An, D. Lv, A. del Campo, and K. Kim, *Nature Communications* **7**, 12999 (2016).
- [31] A. Suresh, V. Varma, P. Batra, and T. S. Mahesh, *The Journal of Chemical Physics* **159**, 024202 (2023).
- [32] C. Zener and R. H. Fowler, *Proceedings of the Royal Society of London. Series A, Containing Papers of a Mathematical and Physical Character* **137**, 696 (1932).
- [33] B. i. e. i. f. m. c. Çakmak and O. E. Müstecaplıoğlu, *Phys. Rev. E* **99**, 032108 (2019).
- [34] O. Abah and M. Paternostro, *Phys. Rev. E* **99**, 022110 (2019).
- [35] T. Guff, S. Daryanoosh, B. Q. Baragiola, and A. Gilchrist, *Phys. Rev. E* **100**, 032129 (2019).
- [36] I. S. Oliveira, T. J. Bonagamba, R. S. Sarthour, J. C. Freitas, and E. R. deAzevedo, in *NMR Quantum Information Processing*, edited by I. S. Oliveira, T. J. Bonagamba, R. S. Sarthour, J. C. Freitas, and E. R. deAzevedo (Elsevier Science B.V., Amsterdam, 2007) pp. 137–181.
- [37] D. G. Cory, M. D. Price, and T. F. Havel, *Physica D: Nonlinear Phenomena* **120**, 82 (1998), proceedings of the Fourth Workshop on Physics and Consumption.
- [38] N. Khaneja, T. Reiss, C. Kehlet, T. Schulte-Herbrüggen, and S. J. Glaser, *Journal of Magnetic Resonance* **172**, 296 (2005).
- [39] J. Zhang, A. M. Souza, F. D. Brandao, and D. Suter, *Phys. Rev. Lett.* **112**, 050502 (2014).
- [40] X. Wang, C.-S. Yu, and X. Yi, *Physics Letters A* **373**, 58 (2008).
- [41] T. B. Batalhão, A. M. Souza, R. S. Sarthour, I. S. Oliveira, M. Paternostro, E. Lutz, and R. M. Serra, *Phys. Rev. Lett.* **115**, 190601 (2015).
- [42] H. T. Quan, Y.-x. Liu, C. P. Sun, and F. Nori, *Phys. Rev. E* **76**, 031105 (2007).